PERGAMON

International Journal of Heat and Mass Transfer 42 (1999) 2455–2464

International Journal of HEAT and MASS TRANSFER

The effect of steady streamwise surface temperature variations on vertical free convection

D.A.S. Rees*

Department of Mechanical Engineering, University of Bath, Claverton Down, Bath BA2 7AY, U.K.

Received 3 October 1997; in final form 27 July 1998

Abstract

We examine how the steady free convective boundary-layer flow induced by a vertical heated surface is affected by the presence of sinusoidal surface temperature variations about a constant mean value which is above the ambient fluid temperature. The problem is studied using fully numerical techniques and an asymptotic analysis which is valid at large distances from the leading edge. The surface rate of heat transfer eventually alternates in sign with distance from the leading edge, but no separation occurs unless the amplitude of the thermal modulation is sufficiently high. The agreement between the numerical results and a two-term asymptotic analysis is excellent.

Nomenclature

a surface temperature wave amplitude
a_2, b_1 constants
A_0, A_1 inner layer functions of ζ
B_0, B_1 inner layer functions of ζ
C_0, C_1 inner layer functions of ζ
d half the dimensional thermal wavelength
f, f_0, f_1 coefficient functions for the streamfunction in the outer layer
F, F_0, F_1 coefficient functions for the streamfunction in the inner layer
g, g_0, g_1 coefficient functions for the temperature in the outer layer
g^* gravity
G, G_0, G_1 coefficient functions for the temperature in the inner layer
$Gr = g^*\beta\Delta T d^3/\nu^2$ Grashof number
p pressure
T temperature
u, v fluid velocities in the x- and y-directions, respectively
x, y streamwise and cross-stream Cartesian coordinates.

Greek symbols
α thermal diffusivity
β coefficient of cubical expansion
ΔT mean temperature drop
ζ, η similarity variable
θ temperature
ν viscosity
ρ reference density
$\sigma = \nu/\alpha$ Prandtl number
ψ streamfunction.

Subscripts
x, y differentiation with respect to x and y, respectively
w refers to the wall
∞ ambient.

Superscript
$'$ differentiation with respect to η or ζ.

1. Introduction

This paper describes an investigation of the effects of surface temperature variations on the steady boundary-layer flow of a Newtonian fluid from a heated vertical surface. It is well-known that power-law surface temperature distributions (and also power-law surface heat fluxes) give rise to self-similar boundary-layer flows [1,

* Tel.: 00 44 1225 826775; fax: 00 44 1225 826928; e-mail: ensdasr@bath.ac.uk

0017–9310/99/$ - see front matter
PII: S0017–9310(98)00304–4

2]. But here we are interested in another form of surface variation, namely, sinusoidal variations about a mean temperature which is held above the ambient temperature of the fluid. This type of surface distribution may be taken to model the effects of a periodic array of heaters behind or within the wall. Although an accurate analysis of such a configuration would require a detailed examination of the effects of solid conduction within the heated surface, it is the aim of the present work to simplify the problem by imposing a surface temperature distribution. In this way we can determine a large amount of information about the resulting flow using both numerical and asymptotic methods.

Various papers have been published which deal with the effects of surface variations. For example, Yao [3] and Moulic and Yao [4, 5] have sought to investigate the effects of streamwise surface undulations of free and mixed convection from vertical surfaces held at uniform temperatures. More recently, Chiu and Chou [6], Hossain et al. [7] and Kim [8] have extended these analyses to micropolar fluids, magnetohydrodynamic convection and non-Newtonian convection, respectively. In a series of papers Rees and Pop [9–13] and Rees [14] have also considered a large variety of analogous flows in porous media. Of these, only [14] has been concerned with the effect of sinusoidal surface temperature variations, although in that case the surface variations were spanwise, thereby giving rise to a three-dimensional flow-field.

The present paper considers in detail how sinusoidal surface temperature profiles in the streamwise direction modify the otherwise self-similar boundary-layer flow. We tackle this topic using both numerical and asymptotic methods. Solutions are presented in terms of the surface rate of heat transfer and shear stress and detailed isotherms are also given. An important feature of the flow is that a near-wall layer develops at large distances downstream of the leading edge. The numerical evidence suggests and the asymptotic analysis shows, that this inner layer decreases in thickness with distance downstream. In this regard it is quite unlike the analogous problem with spanwise temperature variations [15], or the porous medium analogue problems with streamwise [16] or spanwise [14] variations, where the near-wall layer has constant thickness. We find that a two-term asymptotic analysis yields extremely good approximations to the numerical simulations even at distances which are relatively close to the leading edge.

2. Governing equations and boundary-layer analysis

We consider the boundary layer induced by a heated semi-infinite surface immersed in an incompressible Newtonian fluid. In particular, the heated surface is maintained at the steady temperature,

$$T = T_\infty + (T_w - T_\infty)(1 + a\sin(\pi \hat{x}/d)) \tag{1}$$

where T_∞ is the ambient fluid temperature, T_w is the mean surface temperature with $T_w > T_\infty$, a is the relative amplitude of the surface temperature variations and $2d$ is the wavelength of the variations. After a suitable non-dimensionalisation the steady two-dimensional equations of motion are given by

$$u_x + v_y = 0 \tag{2a}$$

$$uu_x + vu_y = -p_x + Gr^{-1/2}(u_{xx} + u_{yy}) + \theta \tag{2b}$$

$$uv_x + vv_y = -p_y + Gr^{-1/2}(v_{xx} + v_{yy}) \tag{2c}$$

$$u\theta_x + v\theta_y = \sigma^{-1}Gr^{-1/2}(\theta_{xx} + \theta_{yy}) \tag{2d}$$

where Gr is the Grashof number and σ is the Prandtl number. In the derivation of equations (2) the Boussinesq approximation has been assumed. We note that the Grashof number has been based on d, half the dimensional wavelength of the thermal waves.

When the surface temperature is uniform and the Grashof number is very large, the resulting boundary-layer flow is self-similar. But the presence of sinusoidal surface temperature distributions, such as that given by (1), renders the boundary-layer flow nonsimilar. The boundary-layer equations are obtained by introducing the scalings

$$u = u^*, \quad v = Gr^{-1/4}v^*, \quad x = x^*,$$
$$y = Gr^{-1/4}y^*, \quad p = Gr^{-1/2}p^*, \quad \theta = \theta^* \tag{3}$$

into equations (2), formally letting Gr become asymptotically large and retaining only the leading order terms. Thus, we obtain

$$u_x + v_y = 0 \tag{4a}$$

$$uu_x + vu_y = u_{yy} + \theta \tag{4b}$$

$$uv_x + vv_y = -p_y + v_{yy} \tag{4c}$$

$$u\theta_x + v\theta_y = \sigma^{-1}\theta_{yy} \tag{4d}$$

where the asterisk superscripts have been omitted for clarity of presentation. Equation (4c) serves to define the pressure field in terms of the two velocity components and is decoupled from the other three equations. Therefore, we shall not consider it further. As the equations are two-dimensional we define a streamfunction, ψ, in the usual way,

$$u = \psi_y, \quad v = -\psi_x \tag{5}$$

and therefore, (4a) is satisfied automatically. Guided by the familiar self-similar form corresponding to a uniform surface temperature, we use the substitution

$$\psi = x^{3/4}f(\eta, x), \quad \theta = g(\eta, x) \tag{6a,b}$$

where

$$\eta = y/x^{1/4} \tag{6c}$$

is the pseudo-similarity variable. Equations (4b) and (4d) reduce to

$$f''' + g + \tfrac{3}{4} f f'' - \tfrac{1}{2} f' f' + x(f_x f'' - f'_x f') = 0 \quad (7a)$$

$$\sigma^{-1} g'' + \tfrac{3}{4} f g' + x(f_x g' - f' g_x) = 0 \quad (7b)$$

and the boundary conditions are

$$f = 0, \quad f' = 0, \quad g = 1 + a \sin \pi x \quad \text{at} \quad \eta = 0, \quad \text{and} \quad f', g \to 0 \quad \text{as} \ \eta \to \infty. \quad (7c)$$

In equations (7), primes denote derivatives with respect to η.

3. Numerical solutions

The parabolic system of equations (7), is nonsimilar and its numerical solution must be obtained using a marching method. The results presented here were obtained using the Keller box method, introduced by Keller and Cebeci [17] and described in more detail in Cebeci and Bradshaw [18]. After reduction of equations (7) to first-order form in η, the subsequent second-order accurate discretisation based halfway between the grid points in both the η- and x-directions yields a set of nonlinear difference equations which are solved using a multi-dimensional Newton–Raphson iteration scheme. In the present methodology the difference equations are defined within the Fortran code and the iteration matrix, which is the Frechét derivative of the difference equations, is determined using numerical differentiation, rather than being specified explicitly within the code. Such a methodology, though slower in execution than when the matrix is defined explicitly, admits a much faster code development. This has been seen to be especially so in relatively complicated parabolic systems such as that considered in [14].

The results presented in Figs 1 and 2 are based on uniform grids in both coordinate directions. There were 201 gridpoints lying between $\eta = 0$ and $\eta = 20$ and 401 between $x = 0$ and $x = 20$. Convergence at each x-station was assumed when the maximum absolute correction was less than 10^{-8}. We restrict the presentation of our results to three values of the Prandtl number: $\sigma = 0.01$, which is representative of liquid metals, $\sigma = 0.7$ for air and $\sigma = 7$ for water.

Figure 1(a)–(c) shows the evolution with x of $f''(\eta = 0)$, a scaled surface shear stress, for various values of the temperature wave amplitude, a. The corresponding rates of surface heat transfer are shown in Figs 2(a)–(c). Some aspects of the overall behaviour of these curves may be explained by observing that the boundary layer is thinner when the surface temperature is relatively high and thicker when it is low. This arises because relatively high surface temperatures induce relatively large upward fluid velocities, with the consequent increase in the rate entrainment into the boundary layer. This causes, in turn, a thinning of the boundary layer. Thus, we should expect high shear stresses and rates of heat transfer at positions

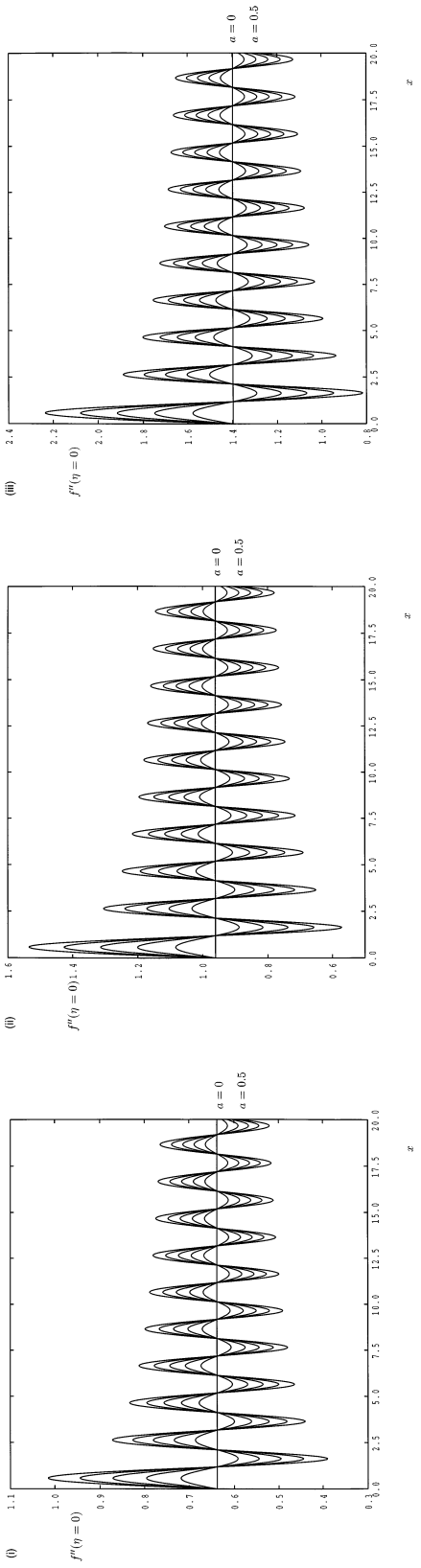

Fig. 1. The evolution with x of the surface shear stress, $f''(\eta = 0)$, for $a = 0$, 0.2, 0.4, 0.6, 0.8 and 1.0 for (i) $\sigma = 0.01$, (ii) $\sigma = 0.7$ and (iii) $\sigma = 7.0$.

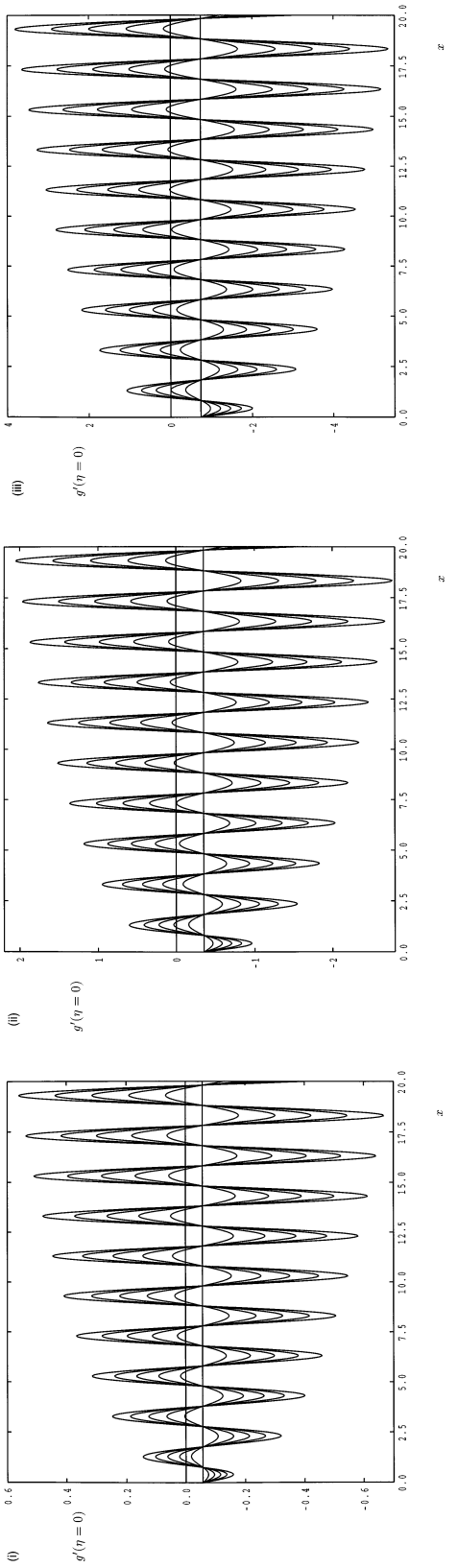

Fig. 2. The evolution with x of the surface rate of heat transfer, $g'(\eta = 0)$, for $a = 0$, 0.2, 0.4, 0.6, 0.8 and 1.0, for (i) $\sigma = 0.01$, (ii) $\eta = 0.7$ and (iii) $\sigma = 7.0$.

or perhaps just beyond where the surface temperature attains its maximum values. There is an obvious qualitative difference between the curves shown in Fig. 1 and those in Fig. 2. As x increases, the amplitude of oscillation of the shear stress curves decays slowly, whereas the amplitude of heat transfer curves increases with x. Indeed, the curves in Fig. 2 suggest that, whatever the value of a, there will always be a value of x beyond which some part of the rate of the heat transfer curve between successive surface temperature maxima will be positive. This somewhat unusual phenomenon for boundary layer flows may be explained by noting that when relatively hot fluid encounters a relatively cold part of the heated surface the overall heat transfer will be from the fluid into the surface, rather than the other way around. However, physical arguments like these are insufficient to account for why the amplitude of oscillation of the curves in Fig. 1 decay, or to give the rate of decay. In the Appendix an asymptotic analysis is presented which gives this quantitative information. Indeed we shall see that the properties of these curves are bound up with the presence of a developing near-wall layer embedded within the main boundary layer.

In Fig. 3 is shown the isotherms for $\sigma = 0.7$ for $a = 0.2$, 0.5 and 1.0. Here we see that the boundary layer maintains its overall thickness in terms of η when x is large, although variations in thickness are clearly present when x is small. The thickness of the region in which strong, surface-induced temperature variations are present reduces slowly in size as x increases. Both of these observations are accounted for in the asymptotic analysis, below. The development of a near-wall layer is most clearly evident by considering the perturbation of the temperature field from that given by $a = 0$. Figure 4 displays such perturbation isotherms for $a = 1.0$ and the presence of the developing near-wall layer is confirmed.

It is necessary to comment on the fact that all the results presented in Fig. 1 have a positive shear stress. It is to be expected that the surface shear stress decreases when the surface temperature is relatively low, since the cool surface is, in effect, slowing the upward progress of the flow. Indeed, Fig. 1 shows that no separation occurs when $a \leqslant 1$ for the range of Prandtl numbers considered. When $a > 1$, however, it is possible to obtain negative shear stresses. We shall not present detailed results, for they depend not only on the value of σ, but also on the phase of surface temperature modulation, an aspect not covered by the present work. However, when $\sigma = 0.7$ incipient separation (i.e. a zero shear stress) first occurs when $a \simeq 1.915$. When $\sigma = 7.0$, the critical value of a is 2.005. This means that the minimum temperature of the 'heated' surface needs to be well below that of the ambient medium before separation can occur. We find that it is not possible to continue numerical integration past the point of separation, a feature which the present problem does not share with that of [10] where integration with

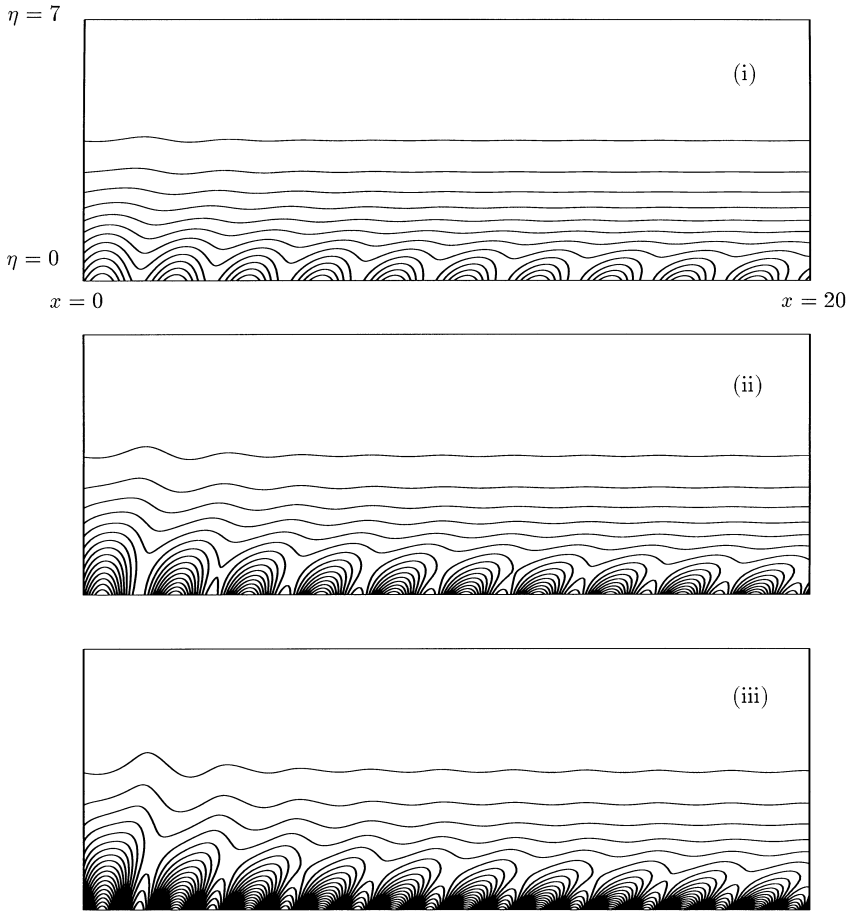

Fig. 3. Isotherms for $\sigma = 0.7$ for (i) $a = 0.2$, (ii) $a = 0.5$ and (iii) $a = 1.0$.

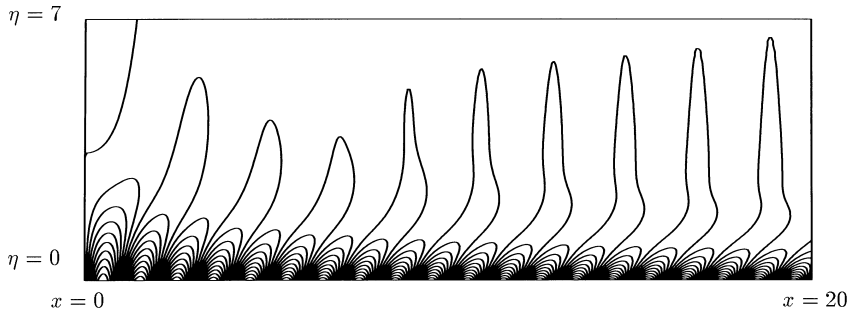

Fig. 4. Perturbation isotherms for $\sigma = 0.7$ and $a = 1.0$. This figure demonstrates the development of a thin near-wall layer as x increases.

ease through successive recirculation bubbles was reported.

The usefulness of the asymptotic analysis contained in the Appendix lies in the facts that (i) it shows that it is impossible to continue the numerical simulations as far as one would wish due to the thinning near-wall layer, (ii) it allows one to terminate the numerical work at a suitable point where the numerical and asymptotic results agree to a high degree of accuracy and (iii) it accounts for the reasons why the flow evolves as it does. For the present flow, the detailed mathematical analysis has been relegated to the Appendix, where it may serve as a model for more complicated flows, such as that of a micropolar fluid under identical circumstances. The results may be

summarised in terms of the surface shear stress and rate of heat transfer:

$$\left.\frac{\partial^2 f}{\partial \eta^2}\right|_{\eta=0} = a_2 - x^{-1/3} a[A_1''(0)\cos \pi x + B_1''(0)\sin \pi x] + O(x^{-2/3}) \quad (8)$$

$$\left.\frac{\partial g}{\partial \eta}\right|_{\eta=0} = x^{1/3} a[A_0'(0)\cos \pi x + B_0'(0)\sin \pi x] + a^2 G_{12s}'(0)\sin 2\pi x + aG_{11c}'(0)\cos \pi x + b_1 + O(x^{-1/3}). \quad (9)$$

In equations (8) and (9) the terms A_0, A_1, B_0, B_1, G_{12s} and G_{11c} refer to functions introduced in the asymptotic analysis. The values of those derivatives given in (8) and (9) may be found in Tables 1 and 2. In Fig. 5 we show comparisons between these asymptotic values and the fully numerical results. Here we take $\sigma = 0.7$ and choose $a = 1$, a very large surface temperature wave amplitude. However, despite the size of a, we see that the curves are in virtually perfect agreement with excellent agreement even for values of x as low as 0.5.

4. Conclusions

A combined numerical and asymptotic analysis of free convection flow from a vertical heated surface with streamwise temperature variations has been undertaken. The numerical results indicate (i) that the effect of sinusoidal thermal modulations is to vary the boundary layer thickness, (ii) that this effect wanes with distance downstream, (iii) that the flow recovers to that of the unmodulated case save for a thin region immediately next to the heated surface where most of the thermal adjustment takes place and (iv) that the rate of heat transfer will eventually alternate in sign with distance irrespective of the amplitude of the thermal modulation. These effects were explained by performing a two-term asymptotic analysis of the governing equations and the existence of a thinning near-wall layer was confirmed and quantified. Detailed comparison between the numerical and asymptotic analyses gave astonishingly good agreement. In addition, it was found that separation did not occur unless $a > 1$, although the precise value of a for incipient separation depends on the value of σ.

Table 1
Values of $f''(0)$, $g'(0)$, A_0' and $B_0'(0)$

σ	$a_2 = f_0''(0)$	$b_1 = g_0'(0)$	$A_0'(0)$	$B_0'(0)$
0.01	1.3969	−0.0570	−0.1286	−0.2227
0.02	1.3562	−0.0789	−0.1605	−0.2779
0.05	1.2844	−0.1200	−0.2139	−0.3704
0.10	1.2150	−0.1627	−0.2647	−0.4581
0.20	1.1329	−0.2177	−0.3258	−0.5639
0.50	1.0086	−0.3120	−0.4255	−0.7363
0.70	0.9601	−0.3532	−0.4684	−0.8104
1.00	0.9082	−0.4010	−0.5179	−0.8960
1.50	0.8492	−0.4607	−0.5799	−1.0030
2.00	0.8079	−0.5066	−0.6278	−1.0858
3.00	0.7508	−0.5767	−0.7015	−1.2130
4.00	0.7113	−0.6304	−0.7584	−1.3114
5.00	0.6814	−0.6746	−0.8055	−1.3926
6.00	0.6574	−0.7123	−0.8460	−1.4624
7.00	0.6375	−0.7455	−0.8816	−1.5239
8.00	0.6206	−0.7752	−0.9136	−1.5790
10.00	0.5928	−0.8268	−0.9694	−1.6754
20.00	0.5119	−1.0052	−1.1638	−2.0105
40.00	0.4392	−1.2146	−1.3945	−2.4076
70.00	0.3866	−1.4104	−1.6117	−2.7813
100.00	0.3559	−1.5495	−1.7668	−3.0478

Table 2
Values of $A_1''(0)$, $B_1''(0)$, $G_{12s}'(0)$ and $G_{11c}'(0)$

σ	$A_1''(0)$	$B_1''(0)$	$G_{12s}'(0)$	$G_{11c}'(0)$
0.01	0.3588	−0.6207	0.07162	0.007757
0.02	0.3477	−0.6015	0.07378	0.011120
0.05	0.3296	−0.5702	0.07792	0.017462
0.10	0.3132	−0.5417	0.08238	0.024087
0.20	0.2942	−0.5090	0.08837	0.032638
0.50	0.2656	−0.4595	0.09930	0.047417
0.70	0.2542	−0.4398	0.10432	0.053938
1.00	0.2418	−0.4183	0.11031	0.061524
1.50	0.2273	−0.3931	0.11799	0.071008
2.00	0.2168	−0.3751	0.12405	0.078301
3.00	0.2020	−0.3495	0.13352	0.089400
4.00	0.1916	−0.3315	0.14096	0.097879
5.00	0.1836	−0.3177	0.14718	0.104817
6.00	0.1772	−0.3065	0.15256	0.110728
7.00	0.1718	−0.2972	0.15734	0.115905
8.00	0.1672	−0.2892	0.16166	0.120525
10.00	0.1597	−0.2762	0.16925	0.128539
20.00	0.1375	−0.2378	0.19614	0.155972
40.00	0.1175	−0.2032	0.22879	0.187820
70.00	0.1031	−0.1783	0.26008	0.217356
100.00	0.0948	−0.1638	0.28266	0.238239

Acknowledgements

The author gratefully acknowledges the validation of the numerical results by the 70 or so final year Computational Fluid Dynamics students who, over the last three years, have solved this numerical problem as their first encounter with nonsimilar boundary-layer flows. The author would like to thank Dr Andrew Bassom,

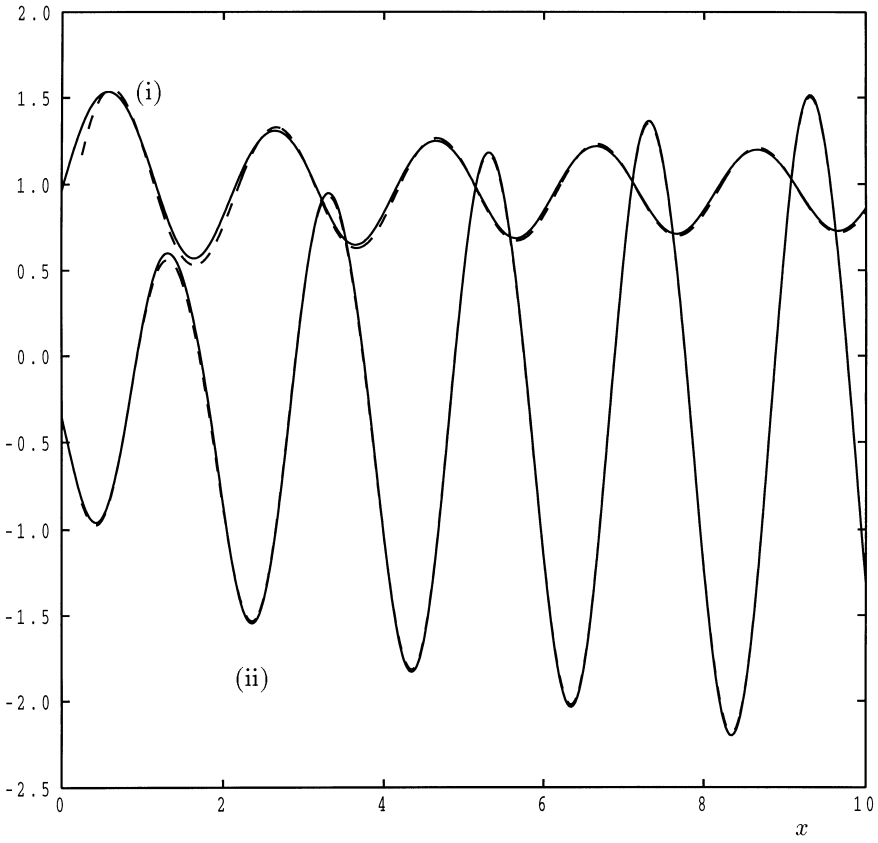

Fig. 5. Comparisons between the fully numerical solution and the asymptotic solutions given by (8) and (9). Here $\sigma = 0.7$ and $a = 1.0$ and comparisons are made between (i) the surface shear stresses and (ii) rates of heat transfer. The solid lines represent the numerical solutions and the dashed lines, the asymptotic solution.

University of Exeter, U.K., for useful comments on the asymptotic analysis.

Appendix: asymptotic analysis

Here we will examine in detail the evolution of the flow at large distances from the leading edge. The main aims are to discover the structure of the flow, to explain all the above-noted observations from the numerical work and to provide correlations for the surface shear stress and rate of heat transfer.

The first task is to determine the thickness of the developing inner (near-wall) layer in terms of η. We begin by following the numerical evidence that the main boundary layer look increasingly like the self-similar $a = 0$ case at large values of x. Thus, we set $f \sim f_0(\eta)$ and $g \sim g_0(\eta)$ in (7) where f_0 and g_0 satisfy the equations

$$f'''_0 + g_0 + \tfrac{3}{4} f_0 f''_0 - \tfrac{1}{2} f'_0 f'_0 = 0 \tag{A1a}$$

$$\sigma^{-1} g''_0 + \tfrac{3}{4} f_0 g'_0 = 0 \tag{A1b}$$

and are subject to the conditions

$$f_0(0) = 0, \quad f'_0(0) = 0, \quad g_0(0) = 1, \quad \text{and} \quad f', g \to 0 \quad \text{as } \eta \to \infty. \tag{A1c}$$

For small values of η we can expand the solutions of (A1) in the power series:

$$f_0 \sim \tfrac{1}{2} a_2 \eta^2 - \tfrac{1}{6} \eta^3 - \tfrac{1}{24} b_1 \eta^4 + \tfrac{1}{480} a_2^2 \eta^5 \tag{A2a}$$

$$g_0 \sim 1 + b_1 \eta - \tfrac{1}{32} \sigma a_2 b_1 \eta^4 + \tfrac{1}{160} \sigma b_1 \eta^5 \tag{A2b}$$

where $a_2 = f''(0)$ and $b_1 = g'(0)$ define the 'constants' a_2 and b_1, and we note that they are both functions of σ. In the inner layer we must balance the order of magnitude of the following terms in equation (7a): the buoyancy term, g, the highest derivative, f''' and the nonlinear terms involving x-derivatives, $x(f_x f'' - f'_x f')$. Given the form of the surface temperature variation, f_x values will vary over an $O(1)$ distance in the x-direction even when $x \gg 1$. Thus, the other nonlinear terms in (7a) are negligible.

Equation (A2a) shows that $f''' = O(1)$ when η is small and this leads us to the scalings, $\eta = O(x^{-1/3})$ and $f = O(x^{-1})$ when x is large. However, this size of η, taken together with the leading behaviour of f_0 in (A2a), shows that $f = O(x^{-2/3})$ in the inner layer. This apparent error in the order-of-magnitude analysis simply indicates that the leading term in the inner layer passively transmits the main layer shear stress to the boundary and it will be independent of x; this is confirmed below. Therefore, the power series expansion in the inner layer must reflect this order-of-magnitude for f.

We shall denote f and g by F and G, respectively, in the inner layer and define a new pseudo-similarity variable ζ, according to

$$\zeta = \eta x^{1/3}. \tag{A3}$$

When ζ is rewritten in terms of x and y, $\zeta = yx^{1/12}$, we can deduce that the inner layer has a physical thickness which is $O(x^{-1/12})$ as x becomes large. Equations (7) are transformed to

$$F''' = x^{-1/3}(\tfrac{3}{4}FF'' - \tfrac{5}{6}F'F') + x^{-1}G + x^{2/3}(F_xF'' - F'_xF') = 0 \tag{A4a}$$

$$\sigma^{-1}G'' + \tfrac{3}{4}x^{-1/3}FG' + x^{2/3}(F_xG' - F'G_x) = 0 \tag{A4b}$$

where primes denote derivatives with respect to ζ when used on inner variables. These equations are supplemented by the initial conditions,

$$F(0) = F'(0) = 0, \quad G(0) = 1 + a\sin\pi x \tag{A4c}$$

but the boundary conditions as $\zeta \to \infty$ have to be obtained by matching with the outer flow solutions of (7a) and (b). Guided by the above scaling arguments we expand the solution of (A4) in the form

$$F = x^{-2/3}F_0 + x^{-1}F_1 + O(x^{-4/3}) \tag{A5a}$$

$$G = G_0 + x^{-1/3}G_1 + O(x^{-2/3}) \tag{A5b}$$

and the solution of (7a,b) in the form

$$f = f_0 + x^{-1/3}f_1 + O(x^{-2/3}) \tag{A6a}$$

$$g = g_0 + x^{-1/3}g_1 + O(x^{-2/3}). \tag{A6b}$$

The equations governing the leading-order inner solutions are

$$F'''_0 = 0, \quad \sigma^{-1}G''_0 + F_{0x}G'_0 - F'_0G_{0x} = 0. \tag{A7a,b}$$

The solution of (A7a) which satisfies the appropriate matching condition obtained from (A2a) is

$$F_0 = \tfrac{1}{2}a_2\zeta^2 \tag{A8}$$

thus, the surface shear stress term has indeed been transmitted unchanged from the outer region. Given that $G_0 = 1 + a\sin\pi x$ at $\zeta = 0$, we need to substitute

$$G_0 = 1 + a[A_0(\zeta)\cos\pi x + B_0(\zeta)\sin\pi x] \tag{A9}$$

into equation (A7b) in order to find the leading-order inner temperature field. Thus, we obtain

$$A''_0 - (a_2\sigma\pi)\zeta B_0 = 0, \quad B''_0 + (a_2\sigma\pi)\zeta A_0 = 0 \tag{A10a,b}$$

subject to the boundary conditions,

$$A_0(0) = 0, \quad B_0(0) = 1, \quad \text{and} \quad A_0, B_0 \to 0 \quad \text{as } \zeta \to \infty. \tag{A10c}$$

We note that $C_0 = A_0 + iB_0$ may be regarded as a complex form of Airy's equation for which the only physically acceptable large-ζ asymptotic behaviour is

$$C_0 \propto \zeta^{-1/4}\exp\left[\frac{2}{3}\left(\frac{-1+i}{\sqrt{2}}\right)\zeta^{3/2}(a_2\sigma\pi)^{1/2}\right] \tag{A11}$$

the other solution having superexponential growth. This result has been used to provide the large-ζ boundary conditions in (A10c). We also note that it is possible to reduce equations (A10a,b) to a canonical form using the substitution $\tilde{\zeta} = (a_2\sigma\pi)^{1/3}\zeta$. Although no advantage is gained at higher-order in the x expansion, it is easy to show that

$$A'_0(0) = -0.36451(a_2\sigma\pi)^{1/3}, \quad B'(0) = -0.63135(a_2\sigma\pi)^{1/3} \tag{A12a,b}$$

by using the substitution together with the classical fourth-order Runge–Kutta scheme allied to the shooting method. The solution of equations (A12) is shown in Fig. 6.

The solutions for A_0 and B_0 and hence G_0, see (A9), decay superexponentially in ζ and therefore, do not affect the main layer, at least to algebraic orders. Therefore, we need now to consider the second-order inner equations,

$$F'''_1 + G_0 = 0, \quad \sigma^{-1}G''_1 + F_{1x}G'_0 - F'_0G_{1x} - F'_1G_{0x} = 0 \tag{A13a,b}$$

subject to

$$F_1 = F'_1 = G_1 = 0 \quad \text{at } \zeta = 0. \tag{A13c}$$

In view of (A9) and the appropriate matching condition obtained from (A2a) we need to set

$$F_1 = -\tfrac{1}{6}\zeta^3 - a[A_1(\zeta)\cos\pi x + B_1(\zeta)\sin\pi x] \tag{A14}$$

into (A13a) to obtain

$$A'''_1 + a_2\pi(B_1 - \zeta B'_1) = A_0, \quad B'''_1 - a_2\pi(A_1 - \zeta A'_1) = B_0. \tag{A15a,b}$$

The boundary conditions at $\zeta = 0$ are

$$A_1 = B_1 = A'_1 = B'_1 = 0. \tag{A15c}$$

The complementary functions of (A14), written in complex form have the following large-ζ asymptotic forms,

$$C_1 = A_1 + iB_1 \propto \zeta, \quad \zeta^{-3/4}\exp\left[\frac{2}{3}\left(\frac{-1+i}{\sqrt{2}}\right)\zeta^{3/2}(a_2\pi)^{1/2}\right]$$

and

$$\zeta^{-3/4}\exp\left[\frac{2}{3}\left(\frac{1-i}{\sqrt{2}}\right)\zeta^{3/2}(a_2\pi)^{1/2}\right] \tag{A15d}$$

given that the superexponentially growing function is

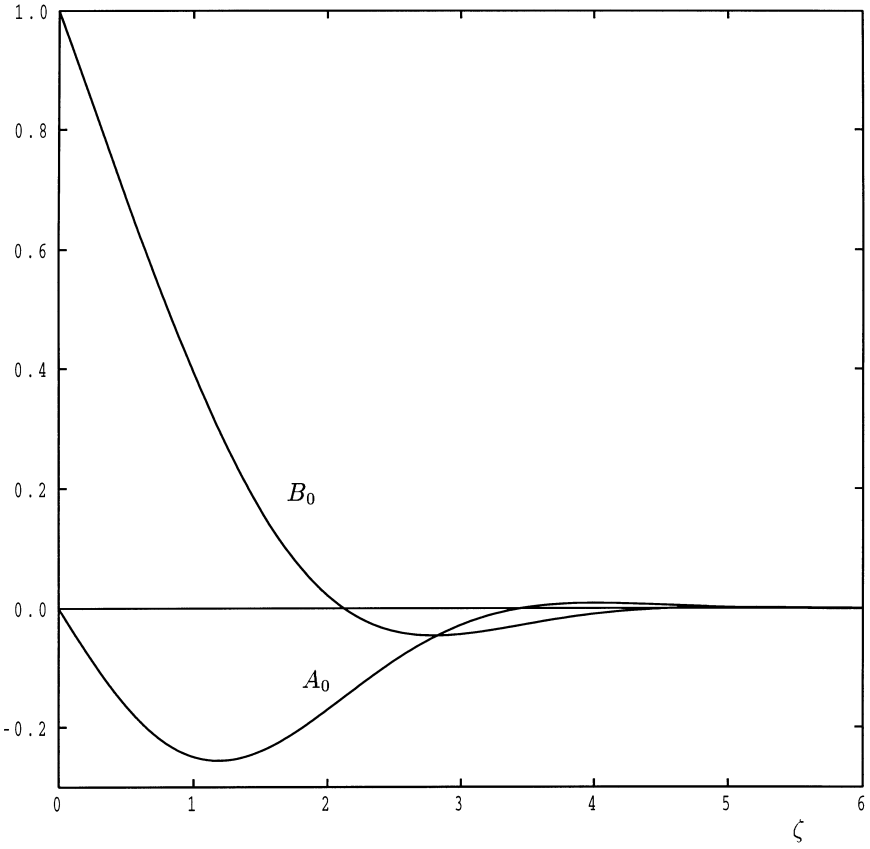

Fig. A1. Solution of equations (A10a) and (A10b).

physically unacceptable, we see that the appropriate boundary conditions for A_1 and B_1 for large ζ are that

$$A_1'', B_1'' \to 0 \quad \text{as } \zeta \to \infty. \tag{A15e}$$

In general then, these inner solutions exhibit linear growth as $\zeta \to \infty$ and this will affect and force further outer flow solutions. Indeed, given the form of (A14), this effect will be x-dependent due to the presence of the $\sin \pi x$ and $\cos \pi x$ terms. If we denote by A_1^∞ and B_1^∞ the asymptotic values of A_1' and B_1' as $\zeta \to \infty$, then

$$F_1 \sim -\tfrac{1}{6}\zeta^3 - a\zeta(A_1^\infty \cos \pi x + B_1^\infty \sin \pi x) \quad \text{as } \zeta \to \infty. \tag{A16a}$$

Therefore, the inner solution obtained so far yields

$$F \sim [\tfrac{1}{2}a_2\zeta^2]x^{-2/3} + [-\zeta^3 - a\zeta(A_1^\infty \cos \pi x + B_1^\infty \sin \pi x)]x^{-1} \tag{A16b}$$

which, when written in outer variables, gives the following matching condition for small values of η,

$$f \sim (\tfrac{1}{2}\eta^2 - \tfrac{1}{6}\eta^3) + [a\eta(A_1^\infty \cos \pi x + B_1^\infty \sin \pi x)]x^{-2/3}. \tag{A17}$$

As this matching condition has no term at $O(x^{-1/3})$ and as the equations for f_1 and g_1 are homogeneous, we conclude that both f_1 and g_1 are zero. The equation for f_2 is now

$$f_{2x}f_0'' - f_{2x}'f_0' = 0 \tag{A18}$$

which may be solved easily to obtain

$$f_2 = -(a/a_2)[A_1^\infty \cos \pi x + B_1^\infty \sin \pi x]f_0'(\eta). \tag{A19}$$

Returning to the second-order inner solution, the substitution of (A8), (A9) and (A14) into (A13b) yields

$$\begin{aligned}&\sigma^{-1}G_1'' - a_2\zeta G_{1x} + \tfrac{1}{2}a^2\pi[B_1'A_0 - B_1A_0' + A_1'B_0 \\ &- A_1B_0']\cos 2\pi x + \tfrac{1}{2}a^2\pi[B_1'B_0 - B_1B_0' - A_1'A_0 \\ &+ A_1A_0']\sin 2\pi x + \tfrac{1}{2}a^2\pi[(A_1B_0)' - (B_1A_0)'] \\ &+ \tfrac{1}{2}a\pi[B_0 \cos \pi x - A_0 \sin \pi x]\zeta^2 = 0.\end{aligned} \tag{A20}$$

The solution of (A20) is effected by first substituting the expression

$$\begin{aligned}G_1 = a^2[&G_{10} + G_{12c}\cos 2\pi x + G_{12s}\sin 2\pi x] \\ &+ a[G_{11c}\cos \pi x + G_{11s}\sin \pi x] + b_1\zeta\end{aligned} \tag{A21}$$

but we omit the presentation of the equations for these five functions of ζ and we note that the very last term in (A21) is required in order to match with the second term of (A2b).

The accurate numerical solution of equations (A15) and those arising from the substitution of (A21) into (A20) prove to be quite difficult to perform using the shooting method due to the presence of unwanted complementary functions with superexponential growth. Thus, these sets of stiff equations were solved using a suitably modified form of the Keller box code described earlier—a direct method. This technique is ideal for such a set of equations, for although the Keller box method was devised originally for solving parabolic marching problems, it is equally well-suited for solving sets of ordinary differential equations. In fact, if the streamwise variable used in the code is taken to be the Prandtl number, then it is very straightforward to obtain solutions over a wide range of values of σ by taking a parameter sweep. A nonuniform grid of 101 points lying between $\zeta = 0$ and $\zeta = 100$ was used for these computations. Richardson's extrapolation was used on results obtained by successive interval-halving of the basic grid to obtain highly accurate solutions.

The shear stresses and rates of heat transfer are of physical interest, but in this section we are also interested in the cross-validation between the asymptotic analysis and the previously described numerical work. Comparison between the numerical and asymptotic requires that the expressions for the asymptotic shear stress and heat transfer are expressed in terms of η-derivatives. Hence, the surface shear stress is

$$\left.\frac{\partial^2 f}{\partial \eta^2}\right|_{\eta=0} = F_0''(\zeta=0) + x^{-1/3}F_1''(\zeta=0) + O(x^{-2/3})$$
$$= a_2 - x^{-1/3}a[A_1''(0)\cos\pi x + B_1''(0)\sin\pi x] + O(x^{-2/3}) \quad \text{(A22)}$$

and the rate of heat transfer is

$$\left.\frac{\partial g}{\partial \eta}\right|_{\eta=0} = x^{1/3}G_0'(\zeta=0) + G_1'(\zeta=0) + O(x^{-1/3})$$
$$= x^{1/3}a[A_0'(0)\cos\pi x + B_0'(0)\sin\pi x] + a^2[G_{10}'(0) + G_{12c}'(0)\cos 2\pi x + G_{12s}'(0)\sin 2\pi x] + a[G_{11c}'(0)\cos\pi x + G_{11s}'(0)\sin\pi x] + b_1 + O(x^{-1/3}). \quad \text{(A23)}$$

Numerically, we find that $G_{10}'(0) = 0$, $G_{12c}'(0) = 0$ and $G_{11s}'(0) = 0$ for all values of σ, which simplifies (A23) slightly, although the functions G_{10}, G_{12c} and G_{11s} are not identically zero. The comparison between the asymptotic results and the numerical simulations has already been presented.

References

[1] S. Ostrach, An analysis of laminar free-convection flow and heat transfer about a flat plate parallel to the direction of the generating body force, NACA TN 2635, 1952.

[2] E.M. Sparrow, J.L. Gregg, Similar solution for free convection from a nonisothermal vertical plate, Trans. ASME Journal of Heat Transfer 80 (1958) 379–384.

[3] L.S. Yao, Natural convection along a vertical wavy surface, Trans. ASME Journal of Heat Transfer 105 (1983) 465–468.

[4] S.G. Moulic, L.S. Yao, Mixed convection along a wavy surface, Trans. ASME Journal of Heat Transfer 111 (1989) 974–979.

[5] S.G. Moulic, L.S. Yao, Natural convection along a vertical wavy surface with uniform heat flux, Trans. ASME Journal of Heat Transfer 111 (1989) 1106–1108.

[6] C.-P. Chiu, H.-M. Chou, Free convection in the boundary layer flow of a micropolar fluid along a vertical wavy surface, Acta Mechanica 101 (1993) 161–174.

[7] M.A. Hossain, K.C.A. Alam, I. Pop, MHD free convection flow along a vertical wavy surface with uniform surface temperature, submitted for publication.

[8] E. Kim, Natural convection along a wavy vertical plate to non-Newtonian fluids, International Journal of Heat Mass Transfer 40 (1997) 3069–3078.

[9] D.A.S. Rees, I. Pop, A note on free convection along a vertical wavy surface in a porous medium, Trans. ASME Journal of Heat Transfer 116 (1994) 505–508.

[10] D.A.S. Rees, I. Pop, Free convection induced by a horizontal wavy surface in a porous medium, Fluid Dynamics Research 14 (1994) 151–166.

[11] D.A.S. Rees, I. Pop, Free convection induced by a vertical wavy surface with uniform heat flux in a porous medium, Trans. ASME Journal of Heat Transfer 117 (1995) 547–550.

[12] D.A.S. Rees, I. Pop, Non-Darcy natural convection from a vertical wavy surface in a porous medium, Transport in Porous Media 20 (1995) 223–234.

[13] D.A.S. Rees, I. Pop, The effect of longitudinal surface waves on free convection from vertical surfaces in porous media, Int. Comm. Heat Mass Transfer 24 (1997) 419–425.

[14] D.A.S. Rees, Three-dimensional free convection boundary layers in porous media induced by a heated surface with spanwise temperature variation, Trans. ASME Journal of Heat Transfer, 1997, to appear.

[15] D.A.S. Rees, Three-dimensional free convection boundary layers induced by a heated surface with spanwise temperature variations, in preparation.

[16] D.A.S. Rees, The effect of streamwise surface temperature variations on vertical free convection in porous media, in preparation.

[17] H.B. Keller, T. Cebeci, Accurate numerical methods for boundary layer flows 1. Two-dimensional flows, Proc. Int. Conf. Numerical Methods in Fluid Dynamics, Lecture Notes in Physics, Springer, New York, 1971.

[18] T. Cebeci, P. Bradshaw, Physical and Computational Aspects of Convective Heat Transfer, Springer, New York, 1984.